Echo-peak shift fails to resolve the liquid-glass phase transition

Lazonder, Kees; Pshenichnikov, Maxim S.; Wiersma, Douwe A.

Published in:
Chemical Physics Letters

DOI:
10.1016/j.cplett.2007.10.069

Publication date:
2007

Available online at www.sciencedirect.com
ScienceDirect
Chemical Physics Letters 449 (2007) 255–259
CHEMICAL PHYSICS LETTERS
www.elsevier.com/locate/cplett

Echo-peak shift fails to resolve the liquid–glass phase transition

Kees Lazonder, Maxim S. Pshenichnikov *, Douwe A. Wiersma

Optical Condensed Matter Group, Zernike Institute for Advanced Materials, University of Groningen, Nijenborgh 4, 9747 AG Groningen, The Netherlands

Received 10 October 2007; in final form 19 October 2007
Available online 25 October 2007

Abstract

The echo-peak shift (EPS) technique, frequently used to study ultrafast solvation dynamics, can be remarkably insensitive to changes in systems' dynamical properties. This is illustrated by comparing the results of EPS and time-resolved photon echo experiments on temperature-dependent optical dephasing in a glass-forming liquid. The observed failure of the EPS technique appears to be a fundamental problem for systems with strong inhomogeneous contribution to the line broadening.

Since its introduction 11 years ago [1–3], the echo-peak shift (EPS) technique has become a benchmark tool for elucidating dynamics at femto- and pico-second time scales. A few examples of its successful applications in physics, chemistry, and biology are studies of solvation dynamics in liquids [2–4] and phospholipid/water interfaces [5], hydrated electron dynamics [6], dynamics of bulk [7–9] and nanoconfined water [10], electron-transfer reactions [11], dynamics and excitation localization in polymers [12–14], energy transfer in bacterial light-harvesting complexes [15–17], and protein dynamics and flexibility [18,19].

The essence of the EPS technique is to measure the time-integrated third-order nonlinear signal, generated in the phase-matched direction $\mathbf{k}_e = \mathbf{k}_3 + \mathbf{k}_2 - \mathbf{k}_1$ (where $\mathbf{k}_i$ stands for the respective wavevector) as a function of the delay t_{12} between the first two excitation pulses E_1 and E_2 (Fig. 1). The EPS is defined as the delay $t_{\mathrm{EPS}} = t_{12}$ where the signal reaches its maximum. If the system under investigation is homogeneously broadened, i.e. the surroundings of the chromophores fluctuate faster than any relevant time scale, then the EPS is zero (normal free induction decay). In contrast, if variations of the chromophore surroundings cause quasi-static frequency offsets (the inhomogeneous broadening), the signal will be retarded with respect to the last excitation pulse, which is known as the photon echo phenomenon [20].

The fact that the EPS is a sensitive indicator of the balance between homogeneous and inhomogeneous contributions to the transition line shape, was recognized in the early days of ultrafast spectroscopy [21,22]. However, it took an additional decade of advances in ultrafast technology [23] as well as development of the multimode brownian oscillator (MBO) theory [24], before it was demonstrated [1–3] that EPS as a function of waiting time t_{13} is directly proportional to the so-called system–bath correlation function (CF):

$$M(t) = \frac{\langle \delta\omega(0) \cdot \delta\omega(t) \rangle}{\langle \delta\omega^2(t) \rangle} \tag{1}$$

Here, $\delta\omega(t)$ is the time-fluctuating contribution of the transition frequency that makes a random walk through frequency space due to the system–bath interactions [24]. The particular value of the CF relates to the probability of finding the transition frequency averaged over an ensemble at some position within the absorption spectrum at time t, giving its original position at time $t = 0$. The two limiting cases of the CF, $M(t) = 1$ and $M(t) = \delta(t)$, correspond to the idealized situations of the purely inhomogeneously and homogeneously broadened transition, respectively [25].

The EPS technique is usually considered as a quick and simple means of obtaining the system dynamics. Two additional features contributed to its triumph. First, unlike in

* Corresponding author.
E-mail address: M.S.Pchenitchnikov@RuG.nl (M.S. Pshenichnikov).

0009-2614/$ - see front matter © 2007 Elsevier B.V. All rights reserved.
doi:10.1016/j.cplett.2007.10.069

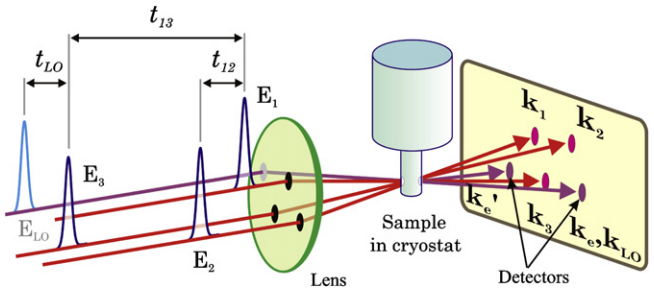

Fig. 1. The experimental arrangement. In the EPS experiment, the echo signals are detected in the conjugated phase-matched directions $\mathbf{k}_e = \mathbf{k}_3 + \mathbf{k}_2 - \mathbf{k}_1$ and $\mathbf{k}'_e = \mathbf{k}_3 - \mathbf{k}_2 + \mathbf{k}_1$ with the local oscillator beam E_{LO} blocked. In the time-resolved echo experiment, the delay t_{LO} of the local oscillator field is scanned while the heterodyned signal is recorded in the $\mathbf{k}_e$ direction.

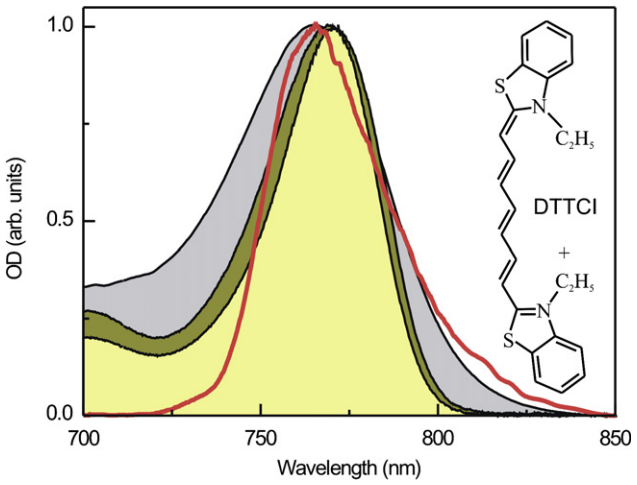

Fig. 2. Absorption spectra of DTTCI in a propanediol–ethanol mixture at 300 K (dark grey shaded), 100 K (dark yellow shaded), and 3 K (light yellow shaded), and the laser excitation spectrum (red curve). For comparison, all spectra are scaled with respect to the 3 K profile. The inset depicts the molecular structure of DTTCI. (For interpretation of the references to color in this figure legend, the reader is referred to the web version of this article).

other photon echo spectroscopies where the echo intensity is obtained [26,27], the observable in the EPS experiment is time. This makes the method relatively insensitive to the laser intensity fluctuations. Second, simultaneous echo detection in the two phase-conjugation directions [28] $\mathbf{k}_e$ and $\mathbf{k}'_e$ (Fig. 1) offers inherent self-referencing of the EPS down to an unprecedented tenths of femtoseconds accuracy, despite environmental perturbations [2,3]. Except for the well-documented malfunction of the EPS at the very short times in the region of pulse overlap [1,3], it is usually regarded to reflect the transient dynamics with respect to the waiting time t_{13}, fairly well.

In this Letter we demonstrate that the EPS experiment completely fails to reveal the fundamental change in solvent dynamics that takes place during the liquid–glass phase transition, while in a time-resolved photon echo experiment the phase transition is clearly discernible. This is unexpected, as both experiments are essentially sensitive to the same physical processes and as such, should yield comparable information. This paradoxical situation is resolved by reassessment of approximations used in the derivation of the EPS expression under conditions of overwhelming inhomogeneity. Our theoretical analysis shows that the EPS insensitivity to the system's dynamics constitutes a general issue for systems where the ratio between homogeneous and inhomogeneous contributions to optical transition, changes in the course of experiment.

Experimentally, the 20 fs pulses produced by a cavity-dumped Ti:Sapphire laser were arranged in the 'box' geometry shown in Fig. 1. The first three pulses E_1, E_2, E_3 were used to generate the photon echo signals detected in the two conjugated phase-matching directions $\mathbf{k}_e$ and $\mathbf{k}'_e$. All beams were focused in the sample using a 125 mm focal length lens which resulted in a focal spot with an ~30-μm diameter. The fourth pulse, E_{LO}, was collinearly mixed with one of the echo beams to time-resolve the temporal echo profile by heterodyning [29,30].

As a sample, a solution of an IR dye 3,3-diethylthiatricarbocyanine iodide (DTTCI) in a glass-forming mixture of 1,2-propanediol and ethanol was used. The absorption spectra of the sample are shown in Fig. 2 for several representative temperatures. With decreasing temperature, the spectral width narrows from ~55 nm at 300 K (grey shaded contour) to ~40 nm at 100 K (dark yellow shaded contour), and further to ~35 nm at 3 K (light yellow shaded contour). The spectrum also exhibits a small red-shift of ~5 nm over the whole temperature range. The laser spectrum was set to match the red wing of the sample absorption to minimize excitation of the higher-frequency vibronic modes at ~700 nm. The sample, with an optical density of ~0.15 at the absorption maximum around 770 nm, was kept at the desired temperature to settle for at least an hour after cooling below the glass temperature of $T_g \approx 150K$ [30] in an Oxford Instruments Variox helium cryostat. To prevent sample heating, pulses with energies as low as ≈500 pJ at a repetition rate of 10 kHz were used.

Fig. 3a shows the experimental temperature dependence of the EPS function. The waiting time of $t_{13} = 210$ fs was set at the first recurrence of the DTTCI dominant vibrational mode at 150 cm^{-1} to provide the vibrational mode suppression regime [31,32]. It is immediately evident from the higher EPS-values at lower temperatures that the system grows to be more static with cooling. Quantitatively, such behavior can be explained by freezing out translational diffusional degrees of freedom of the solvent. At temperatures below the glass transition at $T_g \approx 150$ K, one would expect the EPS to level off because the diffusional processes have come to a complete standstill at this point. Surprisingly however, the EPS shows no evidence of the glass transition as its value continues to increase at temperatures below the glass transition at the same pace as above the glass transition. From this behavior one might conclude that there are still enough changes in the dynamics of the chromophore surroundings to warrant an inhomogeneity growth.

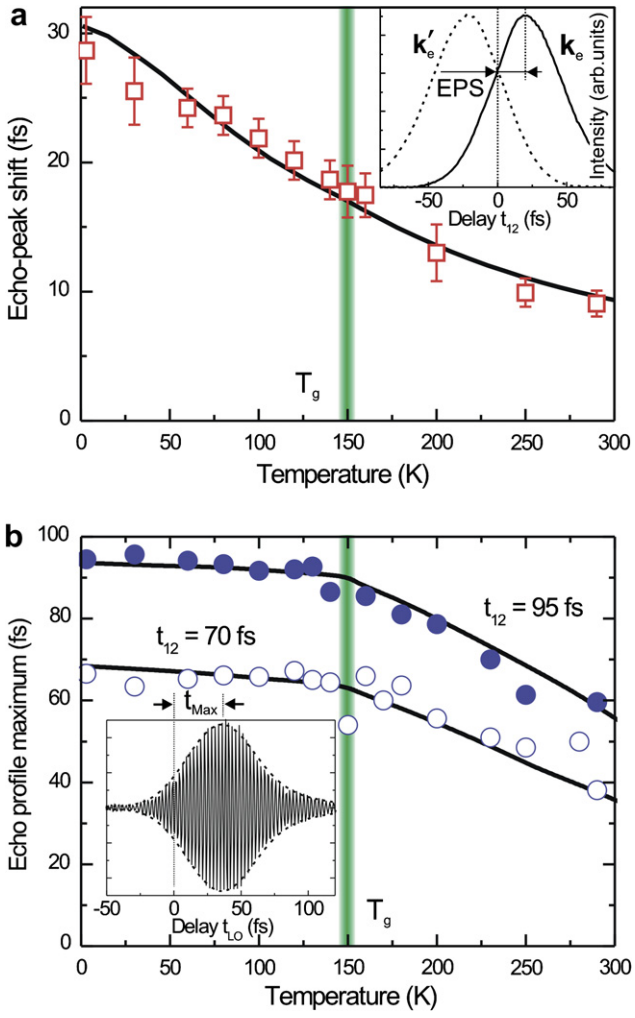

Fig. 3. Temperature dependence of the EPS function (a) and the time-resolved echo maxima positions (b). Symbols show the experimental data points while black solid curves present full-scale calculations as described in the text. The temperature of the glass transition is shown by the shaded contour. The delay t_{12} between the first and third excitation pulses was set at 210 fs in all experiments while the delay t_{12} between the first and second excitation pulses in the time-resolved echo experiments (b) was 70 fs (open circles) and 95 fs (closed circles). Inset in (a): intensities of photon echo signals at the conjugated directions $\mathbf{k}_e$ and $\mathbf{k}'_e$ as functions of the delay time t_{12} between the first excitation pulses at 100 K. Inset in (b): an example of the heterodyned photon echo signal.

To test the possibility of such a conclusion, we time-resolved the transient echo signals. For that, the delay of the weak local oscillator pulse E_{LO} (Fig. 1) was scanned with a fixed delay t_{12} between the first two pulses, to produce an interference pattern with the echo signal (Fig. 3b, inset). After Fourier filtering of the interference fringes, the time position of the echo maximum was determined by fitting of a Gaussian to the echo profile. Fig. 3b shows such positions plotted as a function of temperature for two delay times $t_{12} = 70$ and 95 fs. The glass transition is now clearly discernable as a breaking point at 150 K. From 300 K to the glass temperature, the dynamics slow down in an approximately linear fashion, as is evident from the increased time of the photon echo appearance [2]. Below the glass temperature, the solvent dynamics considerably slow down because of freezing out of the diffusional processes. At the lowest temperatures, the echo maxima are positioned at nearly the same delay as the time t_{12}, indicating the classical Bloch echo [20] behavior, i.e. the mainly static character of the inhomogeneity.

The question arises how the EPS technique, being quite sensitive to solvation dynamics, totally misses the glass transition that drastically changes the dynamical properties of the solvent. To unravel this problem, we review approximations made in obtaining the EPS expression. In contrast to the previous studies on EPS that were primarily concerned with the waiting time dependence (i.e. t_{13}), we focus our attention at the balance between homogeneous and inhomogeneous contributions, while keeping t_{13} a constant.

In the framework of the MBO model, the transient echo intensity in the impulsive excitation limit, is given by the following propagator [24]

$$I_{3PE}(t,t_{23},t_{12}) \propto \left| \left\langle \exp\left\{ -i\int_0^{t_{12}} \delta\omega(t)dt - i\int_{t_{13}}^{t_{13}+t} \delta\omega(t)dt \right\} \right\rangle \right|^2. \quad (2)$$

Following Ref. [2], the correlation function is modeled as a bi-modal function containing fast and slow components:

$$M(t) = (1-a)M_f(t) + aM_s(t), \quad (3)$$

with a being their relative weights. Applying a cumulants expansion [24] to Eq. (2) and extending the correlation function in a Taylor series around t_{13}, one arrives at the following result for the transient echo intensity:

$$I_{3PE}(t,t_{13},t_{12}) \cong \exp[-\Delta^2 \cdot (t_{12}^2 - 2t_{12}taM_s(t_{13}) + t^2)], \quad (4)$$

where $\Delta^2 \equiv \langle \delta\omega^2(t)\rangle/2$ is the absorption spectrum width. The EPS value t_{EPS} at a fixed time t_{13} is found from the zero-crossing point of the derivative of the integral over time t of Eq. (4) with respect to t_{12}:

$$aM_s \exp(-\Delta^2 a^2 M_s^2 t_{EPS}^2) - \Delta t_{EPS}\sqrt{\pi}(1-a^2M_s^2) \times [1 + \mathrm{erf}(\Delta a M_s t_{EPS})] = 0, \quad (5)$$

where $\mathrm{erf}(x)$ is the error function. Next, by assuming that the fast part of the correlation function is dominant, the often used [1–3] expression that establishes the direct proportionality between the EPS and the correlation function, is derived:

$$t_{EPS} = \frac{a}{\Delta\sqrt{\pi}} \cdot M_s. \quad (6)$$

The maximum of the time-resolved (i.e. heterodyned) echo is obtained by differentiating Eq. (4) with respect to the transient time t at a fixed delay t_{12} and finding the zero crossing:

$$t_{max} = at_{12} \cdot M_s. \quad (7)$$

Eqs. (6) and (7) provide similar linear dependences of the EPS and position of the time-resolved echo maximum on parameter a which is the ratio between the fast and slow contributions to the correlation function, and are in contrast with experimental data (Fig. 3). As the time-resolved data (Fig. 3b) are consistent with Eq. (7), our attention is focused at the validity of approximations made upon deriving Eq. (6). To verify those, we numerically solve Eq. (2) with a model correlation function

$$M(t) = (1-a)\exp\left[-\frac{t^2}{2t_0^2}\right] + a, \tag{8}$$

where the fast part is represented by a Gaussian function with characteristic decay time $t_0 = 50$ fs, while the slow part is purely static: $M_s = 1$. Such a correlation function is a reasonable approximation for liquids, as the fast component represents the inertial movement of solvent molecules in the first solvation shell and/or intramolecular wavepacket dynamics, while the slow part is related to slower diffusional processes.

The results of the numerical calculations are presented in Fig. 4. The approximate position of the time-resolved echo maximum given by Eq. (7) (blue circles), follows closely the solution of the complete Eq. (2) (blue thin line). In contrast, the EPS derived directly from Eq. (2) (black curve) exhibits a large divergence from the linear dependence predicted by Eq. (6) (red dashed line) for $a \geqslant 0.5$.

To trace the origin of this deviation, we also calculated the EPS given by Eq. (5) (red squares) that shows excellent correspondence with the complete calculations. Furthermore, in contrast with Ref. [3], Eq. (5) yields reasonable results even if the first-order extension $\mathrm{erf}(x) \cong x$ is used

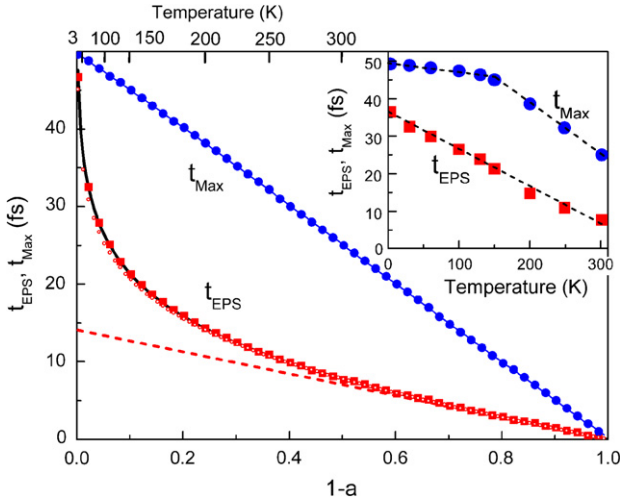

Fig. 4. The results of numerical calculations of the echo-peak shift t_{EPS} from Eq. (2) (black solid curve), Eq. (5) (red squares), Eq. (5) with $\mathrm{erf}(x) \cong x$ (red dotted curve) and Eq. (6) (red dashed line), and position of the time-resolved echo maximum t_{max} from Eq. (2) (blue thin curve) and Eq. (7) (blue circles). The parameters $\Delta = 40$ THz and $t_{12} = 50$ fs are close to their experimental values. The inset shows both t_{EPS} (red squares) and t_{max} (blue circles) as functions of temperature. (For interpretation of the references to color in this figure legend, the reader is referred to the web version of this article).

(red dotted curve in Fig. 4). However, it does not seem possible to simplify the exponential term in Eq. (5) without a catastrophic loss of accuracy for $a \geqslant 0.5$. The reason for this is that for a completely inhomogeneously broadened transition ($aM_s = 1$) the EPS function becomes infinitely large ($t_{EPS} \to \infty$) which prohibits a low-order Taylor expansion. Nonetheless, for practical applications Eq. (5) offers a simple numerical solution, provided that the width of absorption spectrum is known.

The relative insensitivity of EPS to the glass transition can now be explained by its strong nonlinear dependence on the parameter a (i.e. ratio of inhomogeneity/ homogeneity). The time-resolved echo data (Fig. 3b) and Eq. (7) allow a tentative mapping of parameter a on temperature as $a \approx 0.5$ at room temperature and $a \approx 0.85$ at the glass temperature. For the sake of argument, the intermediate variations of a are approximated by linear functions of temperature (Fig. 4, upper scale). Now the calculated EPS values can be presented at a linear temperature scale to facilitate direct comparison with the experimental data in Fig. 3 (Fig. 4, inset).

In the 150 K temperature range above the glass transition, the EPS and position of time-resolved echo maximum are changed quite substantially: by ~10 and ~17 fs, respectively. Below the glass transition the position of time-resolved echo increases by a mere 5 fs for the same temperature interval of ~150 K, because the major solvent dynamics slowdown has already occurred. However, the EPS increases by approximately 10 fs like above the glass transition because of the increased steepness of the EPS as a function of parameter a at its values of $0.8 \leqslant a < 1$. As a result, the glass transition is hardly visible in the EPS data (Fig. 4, inset) which is fully consistent with the experimental data (Fig. 3a). Strictly speaking, the EPS dependence on temperature is not exactly linear; however, the deviations are so minute that they are hardly discernible.

On a final note, the solid curves in Fig. 3 show the results of full-scale calculations that take into account the effects of the finite pulse durations, Stokes shift (that has been ignored so far), as well as the temperature dependence of the MBO model parameters (for details, see Ref. [33]). Both the EPS and echo profile maxima are simulated more than satisfactory, which proves the validity of the model. An additional consideration is that the EPS depends on the absorption spectrum width Δ as shown by Eq. (6). Because the spectrum narrows with decreasing temperature (Fig. 2), a systematic temperature offset adds to the EPS that masks the slowdown of the relevant dynamics. Again, the heterodyned echo experiment does not suffer from this complication.

Summarizing, we have demonstrated that the EPS technique does not resolve a glass–liquid phase transition that dramatically alters solvent dynamics. The reason for this is traced back to the highly nonlinear dependence of the EPS on the balance between the system's homogeneity and inhomogeneity. In contrast to the EPS, the time-resolved echo, as well as its frequency domain counterpart

the two-dimensional correlation spectroscopy [29,30], are more robust techniques for the elucidation of dynamical processes. The increased complexity of the experimental setup is compensated for by a more straightforward data interpretation.

References

[1] W.P. de Boeij, M.S. Pshenichnikov, D.A. Wiersma, Chem. Phys. Lett. 253 (1996) 53.
[2] W.P. de Boeij, M.S. Pshenichnikov, D.A. Wiersma, J. Phys. Chem. 100 (1996) 11806.
[3] M.H. Cho, J.Y. Yu, T.H. Joo, Y. Nagasawa, S.A. Passino, G.R. Fleming, J. Phys. Chem. 100 (1996) 11944.
[4] P. Hamm, M. Lim, R.M. Hochstrasser, Phys. Rev. Lett. 81 (1998) 5326.
[5] H. Bürsing, D. Ouw, S. Kundu, P. Vöhringer, Phys. Chem. Chem. Phys. 3 (2001) 2378.
[6] M.F. Emde, A. Baltuška, A. Kummrow, M.S. Pshenichnikov, D.A. Wiersma, Phys. Rev. Lett. 80 (1998) 4645.
[7] C.J. Fecko, J.D. Eaves, J.J. Loparo, A. Tokmakoff, P.L. Geissler, Science 301 (2003) 1698.
[8] J. Stenger, D. Madsen, P. Hamm, E.T.J. Nibbering, T. Elsaesser, J. Phys. Chem. A 106 (2002) 2341.
[9] S. Yeremenko, M.S. Pshenichnikov, D.A. Wiersma, Phys. Rev. A 73 (2006) 021804.
[10] H.-S. Tan, I.R. Piletic, R.E. Riter, N.E. Levinger, M.D. Fayer, Phys. Rev. Lett. 94 (2005) 057405.
[11] Q.-H. Xu, G.D. Scholes, M. Yang, G.R. Fleming, J. Phys. Chem. A 103 (1999) 10348.
[12] Y. Nagasawa, J.-Y. Yu, M. Cho, G.R. Fleming, Faraday Discuss. 108 (1997) 23.
[13] Y. Nagasawa, K. Seike, T. Muromoto, T. Okada, J. Phys. Chem. A 107 (2003) 2431.
[14] X. Yang, T.E. Dykstra, G.D. Scholes, Phys. Rev. B 71 (2005) 045203.
[15] R. Agarwal, M. Yang, Q.-H. Xu, G.R. Fleming, J. Phys. Chem. B 105 (2001) 1887.
[16] J.M. Salverda et al., Biophys. J. 84 (2003) 450.
[17] H.M. Vaswani, J. Stenger, P. Fromme, G.R. Fleming, J. Phys. Chem. B 110 (2006) 26303.
[18] B.J. Homoelle, M.D. Edington, W.M. Diffey, W.F. Beck, J. Phys. Chem. B 102 (1998) 3044.
[19] R. Jimenez, G. Salazar, J. Yin, T. Joo, F.E. Romesberg, PNAS 101 (2004) 3803.
[20] L. Allen, J.H. Eberly, Optical Resonance and Two-Level Atoms, Wiley, New York, 1975.
[21] S. De Silvestri, A.M. Weiner, J.G. Fujimoto, E.P. Ippen, Chem. Phys. Lett. 112 (1984) 195.
[22] A.M. Weiner, S. De Silvestri, E.P. Ippen, J. Opt. Soc. Am. B 2 (1985) 654.
[23] A.H. Zewail, Femtochemistry: Ultrafast Dynamics of the Chemical Bond, Singapore, 1994.
[24] S. Mukamel, Principles of Nonlinear Optical Spectroscopy, Oxford University Press, NY, USA, 1995.
[25] M. Aihara, Phys. Rev. B 25 (1982) 53.
[26] J.Y. Bigot, M.T. Portella, R.W. Schoenlein, C.J. Bardeen, A. Migus, C.V. Shank, Phys. Rev. Lett. 66 (1991) 1138.
[27] E.T.J. Nibbering, D.A. Wiersma, K. Duppen, Phys. Rev. Lett. 66 (1991) 2464.
[28] D.A. Wiersma, K. Duppen, Science 237 (1987) 1147.
[29] D.M. Jonas, Annu. Rev. Phys. Chem. 54 (2003) 425.
[30] K. Lazonder, M.S. Pshenichnikov, D.A. Wiersma, Opt. Lett. 31 (2006) 3354.
[31] C.J. Bardeen, C.V. Shank, Chem. Phys. Lett. 203 (1993) 535.
[32] W.P. de Boeij, M.S. Pshenichnikov, D.A. Wiersma, J. Chem. Phys. 105 (1996) 2953.
[33] K. Lazonder, M.S. Pshenichnikov, Chem. Phys. in press.